Difference frequency mixing in p-type Si-$Si_{1-x}Ge_x$ heterostructures via intersubband nonlinearities in the far infrared

K.B. Wong and M. Jaros
Department of Physics, Newcastle University, Newcastle Upon Tyne, United Kingdom
(Received 5 July 1994)

We report full-scale psuedopotential calculations concerning the difference frequency mixing in Si-SiGe quantum-well structures. We predict the line shape, the magnitude, and the microscopic origin of the second-order susceptibility. In particular, we establish a link between the strength of the spectra and the degree of asymmetry in the quantum-well system.

I. INTRODUCTION

Si-based semiconductor heterostructures are becoming increasingly important for applications in optoelectronic devices, primarily due to the possibility of designing the valence-band structure where the presence of band mixing effects enhances the optical transitions.[1,2] In fact, the nonlinear effects resulting from virtual excitations between minibands in Si-SiGe structures can be utilized to find applications in the wavelength region of 2–5 and 8–15 μm simply by controlling structural parameters such as well widths and the composition of the SiGe alloy.[3] For example, large second harmonic generation in the mid-infrared to far-infrared range of frequencies has been recently reported.[4] In general, nonlinear second-order susceptibilities associated with transitions within the valence minibands can be strongly enhanced compared to those of bulk semiconductors. Therefore, alternative technologies such as difference frequency mixing can provide additional flexibility for tuning the relevant optical frequency. In this paper, we predict that strong difference-frequency mixing should be observed in narrow p-type SiGe quantum-well structures. The frequency range required for such experiments is well within the reach of a CO_2 laser facility available in most established optics laboratories. Such nonlinear effects have been studied extensively in other materials.[5] We wish to examine in detail the microscopic origin of the optical mixing in connection with the band structure of such materials. Our model quantitatively takes into account the change of symmetry in the crystal, the relativistic spin-orbit effect, and also the strained-induced momentum mixing which are all important to determine new selection rules for optical transitions between valence minibands. This enables us to study the magnitude, directional and frequency dependence of the optical response as well as to hint on designing optimized structures.

II. THEORY

Since the full details of our approach for calculating electronic band structures and evaluating optical response functions are given in the literature,[6,7] here we only focus on the features that differ for this calculation. The process of difference frequency mixing is described by the second-order susceptibility tensor in our calculations. Using the density matrix theory,[8] the following expression for $\chi^{(2)}(-\omega_3;\omega_1,-\omega_2)$ is obtained:

$$\chi^{(2)}_{\mu\alpha\beta}(-\omega_3;\omega_1,-\omega_2)=\frac{ie^3}{Vm^3\epsilon_0\hbar^2 2!\omega_3\omega_1\omega_2}\sum_k\sum_a f_a\sum_{bc}\Bigg[\frac{p^\mu_{ab}p^\alpha_{bc}p^\beta_{ca}}{(\Omega_{ba}-i\Gamma_{ba}-\omega_3)(\Omega_{ca}-i\Gamma_{ca}+\omega_2)}$$
$$+\frac{p^\mu_{ab}p^\beta_{bc}p^\alpha_{ca}}{(\Omega_{ba}-i\Gamma_{ba}-\omega_3)(\Omega_{ca}-i\Gamma_{ca}-\omega_1)}+\frac{p^\beta_{ab}p^\mu_{bc}p^\alpha_{ca}}{(\Omega_{ca}-i\Gamma_{ca}-\omega_1)(\Omega_{bc}+i\Gamma_{bc}+\omega_3)}$$
$$+\frac{p^\alpha_{ab}p^\mu_{bc}p^\beta_{ca}}{(\Omega_{ca}-i\Gamma_{ca}+\omega_2)(\Omega_{bc}+i\Gamma_{bc}+\omega_3)}+\frac{p^\beta_{ab}p^\mu_{bc}p^\alpha_{ca}}{(\Omega_{ba}+i\Gamma_{ba}-\omega_2)(\Omega_{cb}-i\Gamma_{cb}-\omega_3)}$$
$$+\frac{p^\alpha_{ab}p^\mu_{bc}p^\beta_{ca}}{(\Omega_{ba}+i\Gamma_{ba}+\omega_1)(\Omega_{cb}-i\Gamma_{cb}-\omega_3)}+\frac{p^\beta_{ab}p^\alpha_{bc}p^\mu_{ca}}{(\Omega_{ba}+i\Gamma_{ba}-\omega_2)(\Omega_{ca}+i\Gamma_{ca}+\omega_3)}$$
$$+\frac{p^\alpha_{ab}p^\beta_{bc}p^\mu_{ca}}{(\Omega_{ba}+i\Gamma_{ba}+\omega_1)(\Omega_{ca}+i\Gamma_{ca}+\omega_3)}\Bigg],$$

0163-1829/94/50(23)/17328(8)/$06.00

where the component $\chi^{(2)}_{\mu\alpha\beta}(-\omega_3;\omega_1,-\omega_2)$ describes the difference-frequency (i.e., $\omega_3=\omega_1-\omega_2$) polarization induced in the μ direction by incident optical fields at frequencies ω_1 and ω_2 polarized in the α and β directions, respectively. In the equation, $\sum_{abc}$ represents the summation of a,b, and c over all possible states (minibands) at a particular wave vector k. Each combination of abc represents the contribution from the virtual process $a\rightarrow c\rightarrow b\rightarrow a$. Ω_{ij} is the transition frequency between minibands i and j, and p^{δ}_{ij} is the momentum matrix element in the δ direction between i and j. Clearly, for a semiconductor system, the miniband energy separations and momentum matrix elements will have a wave vector dependence, and the expressions for the susceptibilities include a summation over a set of randomly chosen sampling points in the superlattice Brillouin zone $\sum_k$. The Fermi distribution function f_a represents the thermal equilibrium populations of the states. Relaxation processes have been included phenomenologically in the form of the damping terms Γ_{ij} in the frequency denominators of the equation.

III. RESULTS

A. Asymmetric Si-SiGe quantum-well structure

The proposed structure is shown in Fig. 1. The quantum well is made up of 18 $Si_{0.8}Ge_{0.2}$ monolayers and 2 monolayers of $Si_{0.9}Ge_{0.1}$ to form an asymmetric step. The asymmetric structure ensures a large second-order mixing effect due to the lack of inversion symmetry.[9] The barrier of the system consists of 40 monolayers of Si and this layer thickness should be enough to isolate the quantum well. The resulting material is treated in a tetragonal unit cell and the symmetry group is C_{2v}. The structural parameters of the system are chosen for frequency mixing in the range of 30–50 μm. For most applications the pump fields in the optical mixing process lie around the conventional 10.6 μm, therefore, one of the optical transitions involved in the mixing should fall in such a frequency range. In order to have excitations between valence minibands, the system is doped p type to fill the ground state with holes. The charge carriers should be sufficiently dense in order to achieve large second-order nonlinearities. Here we have considered a doping density of 1×10^{19} cm^{-3} which results in a Fermi energy lying 74 meV below the top of the valence-band edge of $Si_{0.8}Ge_{0.2}$. This complicates the choice of structural parameters to obtain transition energies suitable for the long wave length infrared response. The reason is that the single particle approximation in the band structure calculation no longer holds. Instead, a description of the collective transition of carriers, the so-called many-body effect, must be used. To estimate the magnitude of the effect, we consider the conventional exchange and Coulomb interactions given in the literature[10] to correct our transition energies. For the doping concentration mentioned earlier, it results in an upward shift of the top heavy hole state (HH1) by about 25 meV. This energy correction is negligible for other lower lying subbands because the interactions depend upon the number of carriers occupying the subband. More populated subbands will receive more correction than less populated ones. In our doped structure, only the HH1 subband is significantly populated. Apart from the self-energy correction, the coherent many-body system should exhibit the renormalization of intersubband Rabi frequency due to electron-hole Coulomb attractions (i.e., excitonic effects). Such effects may enhance the optical nonlinearities by orders of magnitude compared with predictions of the multilevel susceptibility formula such as that given previously. It is clear that our calculations of $\chi^{(2)}$, which are derived from a system with discrete energy levels, do not give a definitive statement concerning the spectral form of the second-order response.

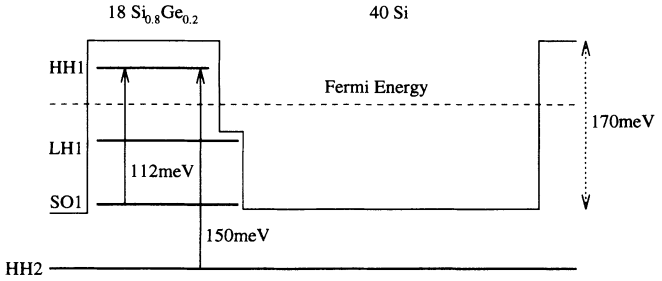

FIG. 1. Schematic energy band diagram of the 18 $Si_{0.8}Ge_{0.2}/2$ $Si_{0.9}Ge_{0.1}/40$ Si quantum-well structure. Zone center transition energies between some of the key states are shown.

In the structure considered, there are another two states localized in the quantum well, namely the light hole state (LH1) and the split-off state (SO1). The energy of the first excited heavy hole state (HH2) lies outside the quantum well, i.e., below the valence-band edge of Si which is the barrier material. We have schematically shown these states together with some of the principal zone center transitions in Fig. 1. At this point we should recall that our objective is to evaluate difference-frequency mixing of 30–50 μm using pump frequencies around 10.6 μm. Thus we look for strong transitions in the band structure with energy separations of 115 and 135 meV.

Accordingly we have calculated the seven independent nonzero components of $\chi^{(2)}(-\omega_3;\omega_1,-\omega_2)$ with $\omega_1=135$ meV and $\omega_2=115$ meV. The results are tabulated in Table I. The largest component is $\chi^{(2)}_{zzz}$. Here z is the

TABLE I. $|\chi^{(2)}_{\mu\alpha\beta}(-\omega_3;\omega_1,\omega_2)|$ for the asymmetric and symmetric Si-SiGe quantum-well structures considered, where $\omega_3=\omega_1-\omega_2$ for frequencies $\omega_1=135$ meV and $\omega_2=115$ meV.

Polarization	Asymmetric	Symmetric
zxx	4.56×10^{-5}	
zxy	5.61×10^{-6}	8.52×10^{-6}
xyz	7.94×10^{-6}	2.60×10^{-6}
xxz	2.69×10^{-5}	
zzz	2.68×10^{-4}	
xzx	4.33×10^{-5}	
xzy	2.42×10^{-6}	2.59×10^{-5}

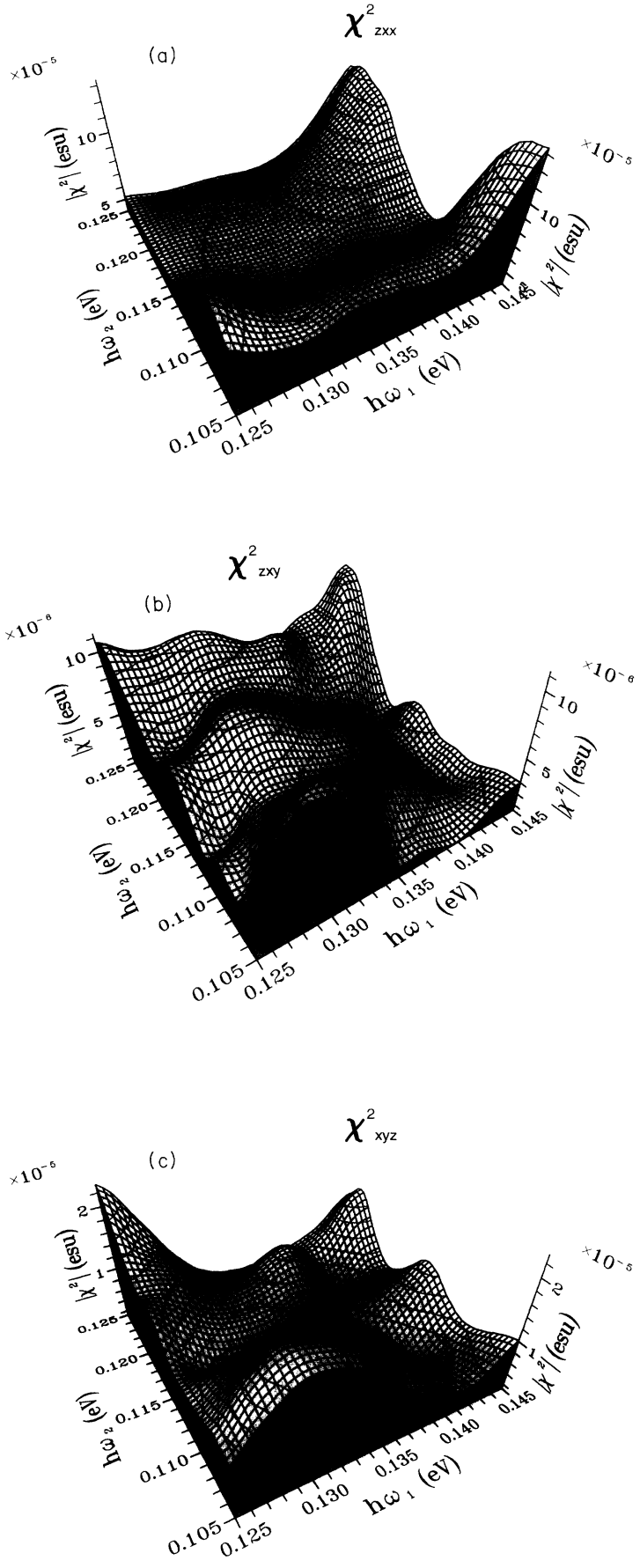

FIG. 2. Three-dimensional surface plots of $|\chi^{(2)}_{\mu\alpha\beta}(-\omega_3;\omega_1,\omega_2)|$ for the asymmetric structure given in Fig. 1, where $\omega_3 = \omega_1 - \omega_2$ for frequencies $\omega_1 = 135$ meV ± 10 meV and $\omega_2 = 115$ meV ± 10 meV. All seven independent nonzero components with different polarization $\mu\alpha\beta$ are shown.

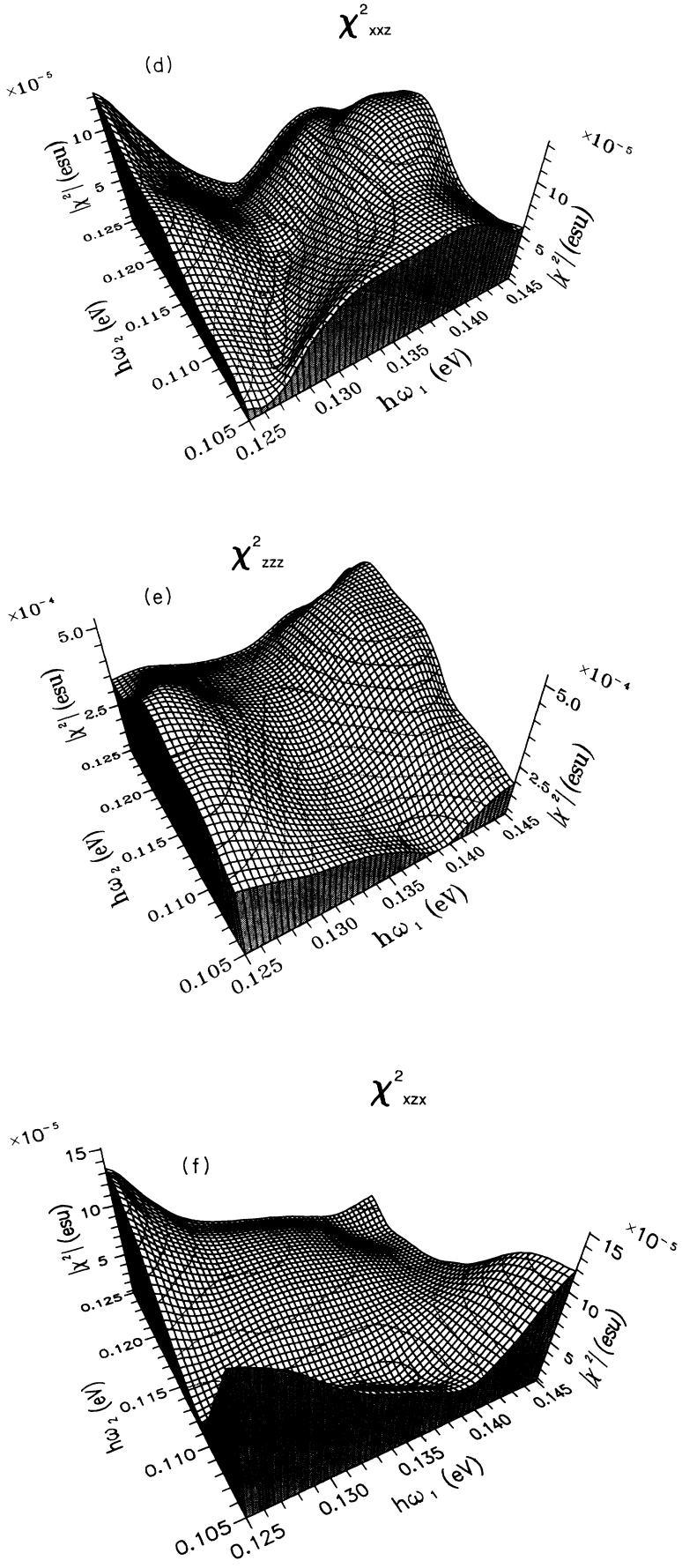

FIG. 2 *(Continued).*

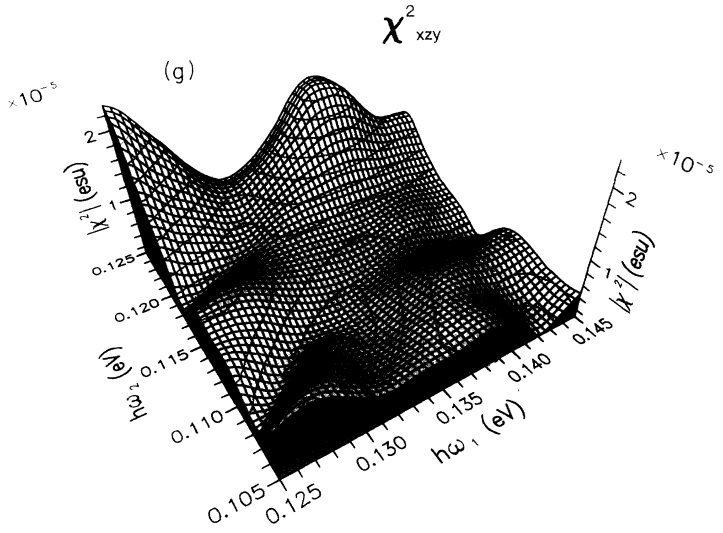

FIG. 2 *(Continued).*

quantum-well growth direction and directions x, y lie in the plane parallel to the quantum-well layers. We also find that the component $\chi^{(2)}_{zxx}$ is large. $\chi^{(2)}_{zxx}$ describes an induced polarization in the z direction in response to fundamental fields applied in the x direction. This component is, therefore, particularly useful for laser inputs at normal incidence, which was otherwise believed to be impossible in the past. To assess for the optimization of the response, more calculations have been performed as we vary the frequencies of the applied fields for $\omega_1 = 135$ meV ± 10 meV and $\omega_2 = 115$ meV ± 10 meV. The results are presented in Fig. 2(a)–(g) for different tensorial components of $\chi^{(2)}(-\omega_3; \omega_1, -\omega_2)$. The dependence of $\chi^{(2)}$ on frequencies of ω_1 and ω_2 can be understood from the band structure as both the energies and the strength of the responsible optical transitions vary over the Brillouin zone.

Next, it is instructive to discuss the origin of the second-order response, i.e., to identify the key transitions that are responsible for the difference-frequency mixing. Let us refer to Fig. 1 again. The transitions involved in the mixing are HH1→SO1 and HH2→HH1. Transition between states HH1 and SO1 is partially allowed because of valence-band mixing. It is noted that the zone center transitions do not correspond to the mixing of frequencies at 115 meV and 135 meV. However, away from the Brillouin zone center there exists transitions at these energies. To further explain the obtained results we present, in Fig. 3, the band structure of the system along two symmetry lines in the Brillouin zone. We can see that transitions at A and B contribute to the process HH2→HH1→SO1→HH2 for mixing frequencies of 115 meV and 135 meV. It is worth pointing out that the difference-frequency mixing at the above frequencies (this corresponds to the center positions of the three-dimensional pictures in Fig. 2) cannot be easily optimized. This is because state HH2 is essentially a continuum state and has a large miniband width. Such a band structure effect manifests itself in the directional dependence of the optical mixing. It follows that different tensorial components of $\chi^{(2)}$ do not necessarily peak at the same position (see Fig. 2).

B. The role of asymmetry in Si-SiGe quantum-well structures

From the previous section we conclude that large optical second-order nonlinearities can be achieved in an asymmetric Si-SiGe quantum-well structure. The next step is to investigate the role of asymmetry on the optical mixing. It is well known that $\chi^{(2)}$ is subject to certain symmetry restrictions, for instance the tensor is strictly zero for those crystal classes that have inversion symmetry. In a symmetric quantum-well structure the symmetry group is D_{2d}, and so there are only three nonzero independent components of $\chi^{(2)}$, namely $\chi^{(2)}_{xyz}$, $\chi^{(2)}_{zxy}$, and

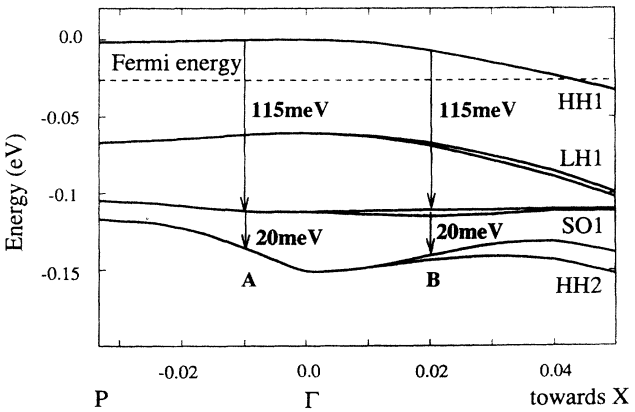

FIG. 3. Miniband structure of the asymmetric Si-$Si_{0.8}Ge_{0.2}$ quantum-well structure along the P-Γ and Γ-X (i.e., Δ line in bulk) symmetry lines. The scale shown along these lines is measured in unit of $2\pi/a$ where a is the bulk lattice constant of the structure. P is the edge of the minizone along the quantum-well growth direction (z).

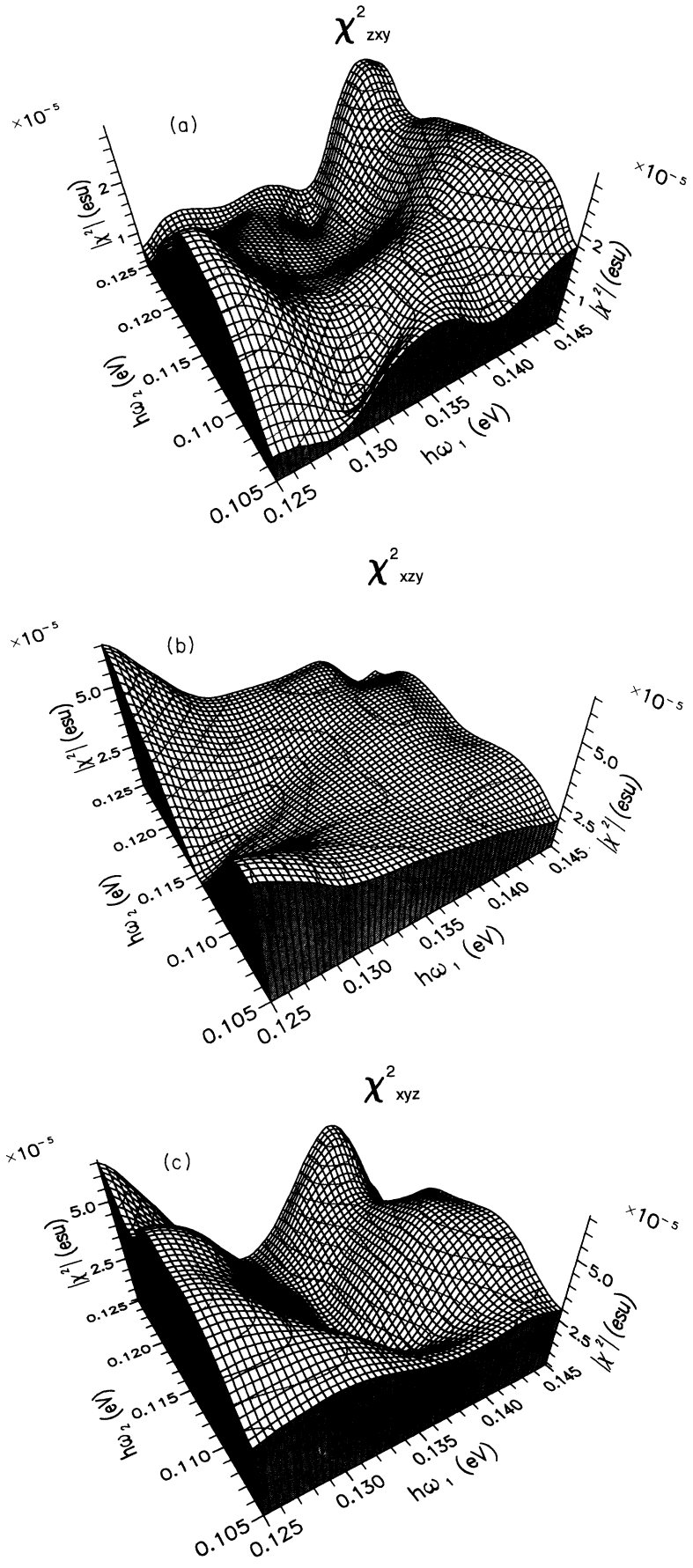

FIG. 4. All three independent nonzero components of $|\chi^{(2)}_{\mu\alpha\beta}(-\omega_3;\omega_1,\omega_2)|$ for the symmetric Si-$Si_{0.8}Ge_{0.2}$ quantum-well structure.

$\chi^{(2)}_{xzy}$. This indicates that the largest component ($\chi^{(2)}_{zzz}$) that existed in the asymmetric quantum-well structures vanishes in this case because of crystal symmetry. This is considered as a major drawback in symmetric well structures in the past if one is interested in the nonlinearities associated with the excitations between conduction minibands in an n-type material. This is because, owing to the selection rule of the Γ conduction band, all the other components of $\chi^{(2)}$ are usually very small. However, one might hope to circumvent such problems in a p-type symmetric well structure. It should be stressed that our band structure and momentum matrix elements are generated in a model that takes into account the crystal symmetry. For instance, a detailed band structure is available over the entire Brillouin zone. Apparently, the angular dependence of momentum matrix elements are determined with quantitative precision. On the basis of these calculations, we can correctly account for any small change in the crystal potential.

To compare in the simplest way with the previous results, we consider a symmetric quantum-well structure of Si-$Si_{0.8}Ge_{0.2}$ by removing the $Si_{0.9}Ge_{0.1}$ alloy layer of the asymmetric structure given in Fig. 1. We have chosen 19 monolayers of $Si_{0.8}Ge_{0.2}$ and 41 monolayers of Si to avoid having an inversion center in the system. This structure has the closest resemblance to the previous asymmetric structure for comparison purpose. The three calculated independent components of $\chi^{(2)}(-\omega_3;\omega_1,-\omega_2)$ with $\omega_1 = 135$ meV and $\omega_2 = 115$ meV are tabulated in Table I and their frequency dependence are presented in Fig. 4. Again we have shown the span of ± 10 meV from the pump frequencies of 115 meV and 135 meV. From these diagrams, we can see that all three components are of magnitude around 10^{-5} esu. We can also directly compare the results with the asymmetric structure. $\chi^{(2)}$ here are obviously larger than their counterparts in the asymmetric structure. To explain this we have to study the processes contributing to $\chi^{(2)}$. We found that the main process is HH2→HH1→SO1→HH2. This process of difference-frequency generation can be summarized in an energy-level description given in Fig. 5. The system first absorbs a photon of frequency ω_1 and jumps to the highest available level HH1. Then it decays by a two-photon emission process that is stimulated by the presence of the ω_2 field, which is already present. In fact, it

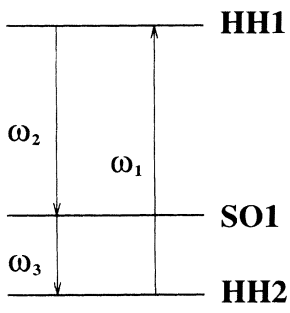

FIG. 5. An energy-level description for the difference-frequency generation.

is the same process contributing to $\chi^{(2)}$ in the asymmetric well structure. Since the transition energies between the concerned states are similar in both cases, the difference in magnitude of $\chi^{(2)}$ must have resulted from the difference in optical transition matrix elements. Therefore, we tabulate the strength for the three optical transitions in concern together with their energies in Table II. The results show that the strength of both transitions HH2→HH1 and SO1→HH2 are larger in the symmetric well case. This seems rather unusual and hence requires further explanations.

Let us write down the optical matrix element in the well-known envelope function model. By considering two states i and f, which are composed of periodic parts u_i, u_f (Bloch functions) and slowly varying parts F_i and F_f (envelope functions), respectively, the optical matrix element can be expressed as

$$\langle u_f|p|u_i\rangle\langle F_f|F_i\rangle \ ,$$

where $\langle F_f|F_i\rangle$ is the overlap integral between the envelope function part and $\langle u_f|p|u_i\rangle$ is the corresponding momentum matrix element defined between the Bloch function part of states i and f. Selection rules for particular transition can be deduced by considering separately $\langle u_f|p|u_i\rangle$ and $\langle F_f|F_i\rangle$. Momentum mixing of the bulk Bloch functions of the confined quantum-well states can, of course, relax the selection rule by enhancing the term $\langle u_f|p|u_i\rangle$. For example, transition HH1→SO1 is allowed because of valence-band mixing between bulk heavy and light hole characters. Asymmetry in the quantum-well potential that we have considered in the previous section can also enhance the momentum mixing. Since mixing occurs in the plane perpendicular to the quantum-well growth direction, the asymmetry considered here can only contribute little to the mixing. On the other hand, the term $\langle F_f|F_i\rangle$ which describes the overlap between the two states, decreases with increasing asymmetry in the structure for obvious reasons.

Using the above arguments, we can easily explain the results in Table II. HH2→HH1 is an allowed transition because both states involved are derived from the same bulk heavy hole band edge and it obeys the selection rule for intersubband transition. Thus the term $\langle u_f|p|u_i\rangle$ is finite and is similar for both symmetric and asymmetric structures. However, the overlap integral in the asymmetric structure is smaller. It follows that the optical matrix element is smaller in this case. For the transition HH1→SO1, momentum mixing enhances the size of $\langle u_f|p|u_i\rangle$ but only to a small extent. $\langle F_f|F_i\rangle$ is small for this transition because both states involved are ground states of the corresponding bulk momentum character. Hence its magnitude is insensitive to the change in symmetry. Finally, transition SO1→HH2 depends on both terms. As state HH2 is a continuum state, the asymmetry has a large effect on determining the size of $\langle F_f|F_i\rangle$ for the transition. The increase of $\langle u_f|p|u_i\rangle$ brought in by enhanced momentum mixing simply cannot compete with the more rapid decrease of $\langle F_f|F_i\rangle$.

Lastly, it is useful to point out that one can generally obtain an increased second-order response by designing structures with a large asymmetry. Such depen-

TABLE II. Squared optical matrix elements and energies for transition at the center of the Brillouin zone in both symmetric and asymmetric Si-$Si_{0.8}Ge_{0.2}$ quantum-well structures. Energies are measured in meV and matrix elements in a.u.

	Symmetric well			Asymmetric well		
Transition	Energy	Polarization x, y	Polarization z	Energy	Polarization x, y	Polarization z
HH1→HH2	152	0.10×10^{-5}	0.90×10^{-2}	150	0.10×10^{-6}	0.20×10^{-2}
HH1→SO1	114	0.32×10^{-4}	0.63×10^{-7}	112	0.66×10^{-4}	0.20×10^{-6}
SO1→HH2	38	0.13×10^{-2}	0.60×10^{-5}	38	0.33×10^{-4}	0.15×10^{-5}

dence of second-order processes on asymmetry has been addressed in our recent publication[11] concerning GaAs-AlAs quantum-well structures. We, therefore, refer our readers to it for more details.

IV. CONCLUSIONS

We have performed a full-scale theoretical study of difference-frequency mixing in p-type Si-SiGe quantum-well structures in the far-infrared range. We demonstrate that large optical response can be obtained in the asymmetric structure where the second-order optical susceptibilities $\chi^{(2)}_{zzz}$ and $\chi^{(2)}_{zxx}$ are both very large. Our analysis of band structure effects shows that steplike structural asymmetry normally invoked to study $\chi^{(2)}$ in quantum wells does not play a significant role in the optical mixing that determines the magnitude of $\chi^{(2)}$.

ACKNOWLEDGMENTS

We would like to thank the United Kingdom Science and Engineering Research Council, the Office of Naval Research (U.S.A.), and ESPRIT-Basic Research European Community Programme for financial support. It is a pleasure to acknowledge stimulating conversations with Dr. Capasso and Dr. Sirtori of AT&T Bell Laboratories which initiated this study.

[1] J. S. Park, R. P. G. Karunasiri, and K. L. Wang, Appl. Phys. Lett. **61**, 681, 1992.
[2] T. Fromherz, E. Koppensteiner, M. Helm, G. Bauer, J. F. Nützel, and G. Abstreiter, Solid-State Electron. **37**, 941 (1994).
[3] E. Corbin, K. B. Wong, and M. Jaros, Phys. Rev. B **50**, 2339 (1994).
[4] M. J. Shaw, K. B. Wong, and M. Jaros, Phys. Rev. B **48**, 2001 (1993).
[5] C. Sirtori, J. Faist, F. Capasso, D. L. Sivco, and A. Y. Cho, Solid-State Electron. **37**, 1191 (1994).
[6] I. Morrison, M. Jaros, and K. B. Wong, Phys. Rev. B **35**, 9693 (1987).
[7] M. J. Shaw, D. Ninno, B. M. Adderley, and M. Jaros, Phys. Rev. B **45**, 11 031 (1992).
[8] P. N. Butcher and D. Cotter, *The Elements of Nonlinear Optics* (Cambridge University Press, Cambridge, 1990).
[9] The inversion symmetry here refers to that of a one-dimensional potential of the quantum well. Strictly speaking, there is no center of inversion even in a symmetric well structure where one has an odd number of monolayers of SiGe alloy.
[10] K. M. S. V. Bandara, D. D. Coon, O. Byungsung, Y. F. Lin, and M. H. Francome, Appl. Phys. Lett. **53**, 1931 (1988).
[11] M. A. Cusack, M. J. Shaw, and M. Jaros, Phys. Rev. B **49**, 16 575 (1994).

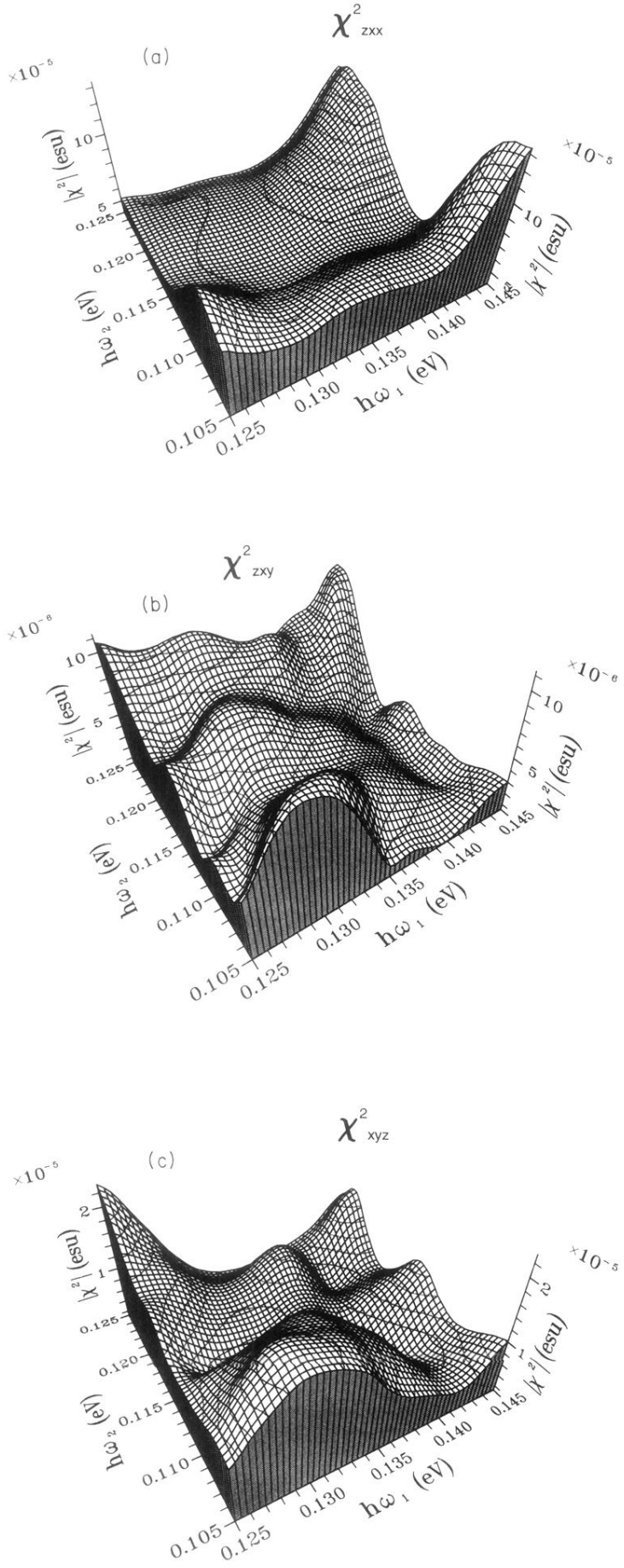

FIG. 2. Three-dimensional surface plots of $|\chi^{(2)}_{\mu\alpha\beta}(-\omega_3;\omega_1,\omega_2)|$ for the asymmetric structure given in Fig. 1, where $\omega_3 = \omega_1 - \omega_2$ for frequencies $\omega_1 = 135$ meV ± 10 meV and $\omega_2 = 115$ meV ± 10 meV. All seven independent nonzero components with different polarization $\mu\alpha\beta$ are shown.

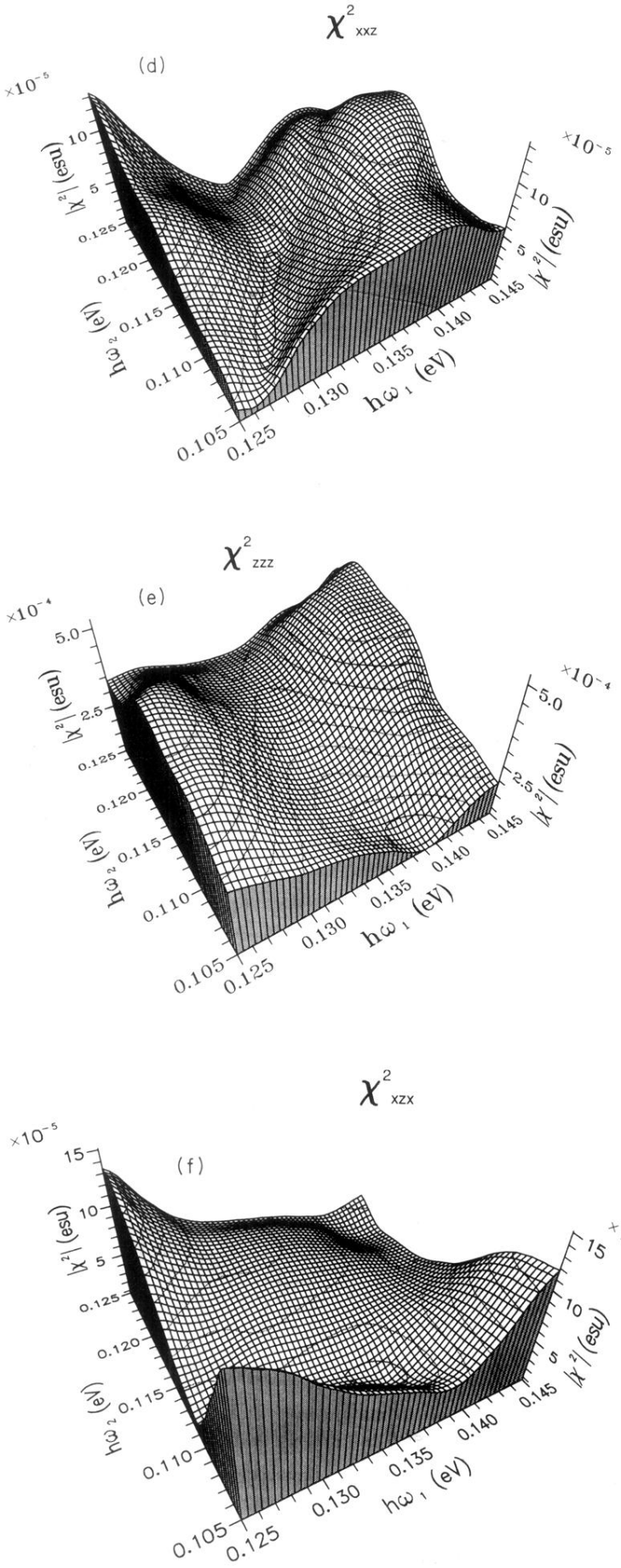

FIG. 2 *(Continued).*

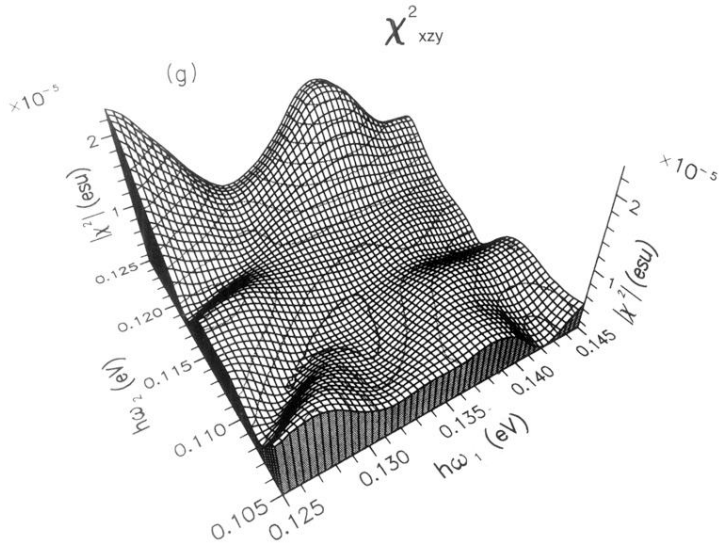

FIG. 2 *(Continued).*

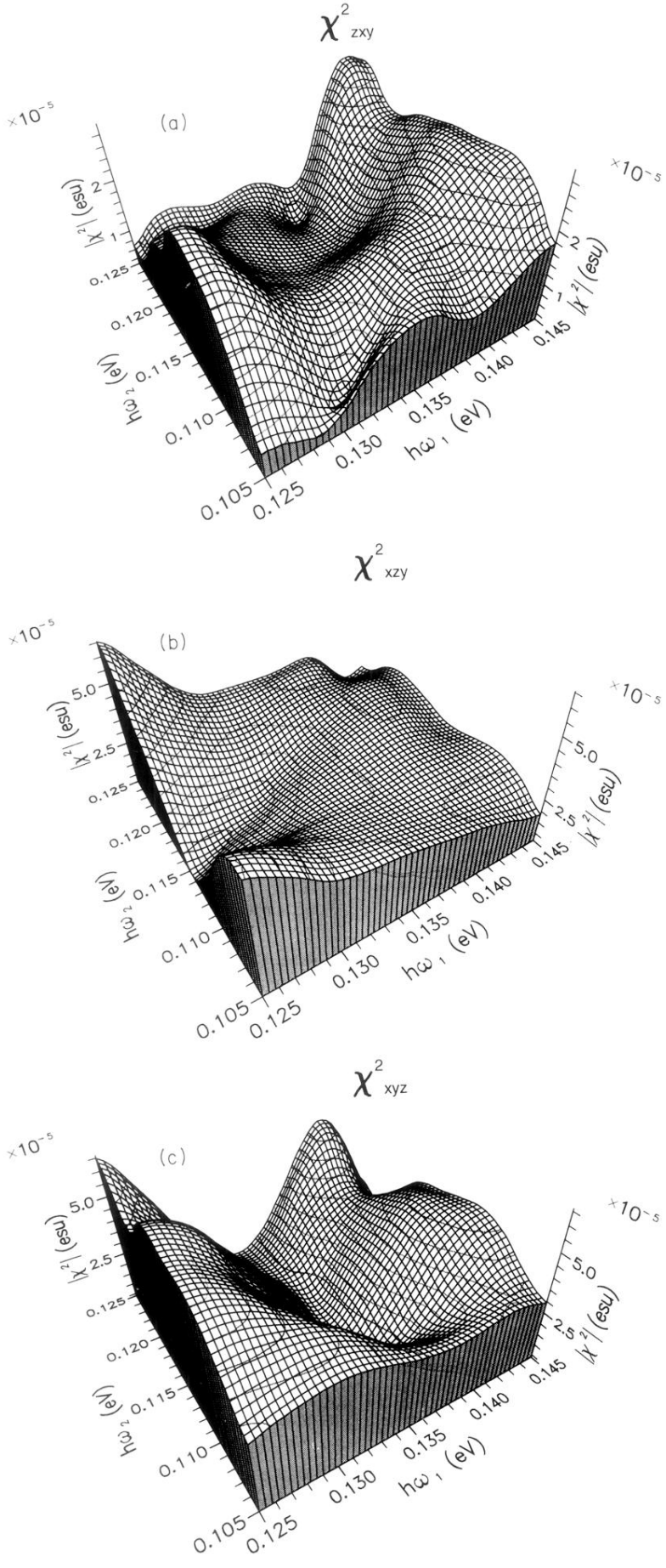

FIG. 4. All three independent nonzero components of $|\chi^{(2)}_{\mu\alpha\beta}(-\omega_3;\omega_1,\omega_2)|$ for the symmetric Si-$Si_{0.8}Ge_{0.2}$ quantum-well structure.